A&A 475, 1027–1037 (2007)
DOI: 10.1051/0004-6361:20078196
© ESO 2007

Astronomy & Astrophysics

Variations of the high-level Balmer line spectrum of the helium-strong star σ Orionis E*

M. A. Smith[1,★★] and D. A. Bohlender[2]

[1] Department of Physics, Catholic University of America, Washington, DC 20064, USA
e-mail: msmith@stsci.edu
[2] National Research Council of Canada, Herzberg Institute of Astrophysics, 5071 W. Saanich Rd., Victoria, BC V9E 2E7, Canada

Received 30 June 2007 / Accepted 18 September 2007

ABSTRACT

Using the high-level Balmer lines and continuum, we trace the density structure of two magnetospheric disk segments of the prototypical Bp star σ Orionis E (B2p) as these segments occult portions of the star during the rotational cycle. High-resolution spectra of the Balmer lines ≥H9 and Balmer edge were obtained on seven nights in January–February 2007 at an average sampling of 0.01 cycles. We measured equivalent width variations due to the star occultations by two disk segments 0.4 cycles apart and constructed differential spectra of the migrations of the corresponding absorptions across the Balmer line profiles. We first estimated the rotational and magnetic obliquity angles. We then simulated the observed Balmer jump variation using the model atmosphere codes *synspec/circus* and evaluated the disk geometry and gas thermodynamics. We find that the two occultations are caused by two disk segments. The first of these transits quickly, indicating that the segment resides in a range of distances, perhaps 2.5−6 R_*, from the star. The second consists of a more slowly moving segment situated closer to the surface and causing two semi-resolved absorbing maxima. During its transit this segment brushes across the star's "lower" limb. Judging from the line visibility up to H23-H24 during the occultations, both disk segments have mean densities near 10^{12} cm^{-3} and are opaque in the lines and continuum. They have semiheights less than $\frac{1}{2}$ R_*, and their temperatures are near 10 500 K and 12 000 K, respectively. In all, the disks of Bp stars have a much more complicated geometry than has been anticipated, as evidenced by their (sometimes) non-coplanarity, de-centerness, and from star to star, differences in disk height.

Key words. stars: individual: σ Orionis E – stars: magnetic fields – stars: circumstellar matter – stars: winds, outflows – stars: early-type – ultraviolet: stars

1. Introduction

Over the last several years the interest in the class of magnetic Bp stars has spurred the accumulation of datasets at many wavelengths over the stars' rotational/magnetic cycles. These datasets support the view that the circumstellar environment is the site of a balance of physical processes that channels the wind toward the magnetic plane. If the magnetic field is strong, that is if the circumstellar magnetic energy density exceeds the wind energy density, the star's wind is channeled into the magnetic plane where a shock is formed and the cooled shock settles to form a stable disk. The magnetic axis is typically inclined with respect to the rotational axis. Then, as different portions of the disk wobble in front of the star during the rotational cycle, they produce alternate absorption and emission components in the Hα, UV resonance lines, and low-excitation metallic lines (e.g., Bohlender et al. 1987; Shore 1987; Bolton 1994). To complicate the picture, it appears that slow infall of disk matter is responsible for producing inhomogeneous metal-poor patches or a belt along the magnetic equator (e.g., Khokhlova et al. 2000; Groote 2003). Also, although there remains a theoretical difficulty with the fractionation hypothesis for helium (Krtička et al. 2006), enough neutral helium atoms in fact seem likely to separate from the polar wind, return to the surface, and accumulate there as helium caps.

Recent theoretical refinements in the picture (e.g., Preuss et al. 2004; Townsend & Owocki 2005, hereafter TO05) suggest that the wind will settle onto low equipotential surfaces determined by the balance of radiative, gravitational, magnetic, and centrifugal forces. These surfaces reside primarily, though not exclusively, in the disk plane. Because the disk is likely to have a nonaxisymmetric density distribution, we will refer to the accumulations near the plane responsible for time-variable spectral features as disk segments. TO05 have presented a "rigidly rotating magnetospheric" ab initio model to explain physical properties of these segments for the case of σ Ori E and it can be applied to the cases of other Bp stars with arbitrary magnetic inclinations and viewed from any rotational inclinations. TO05 find that the disk plane is not precisely perpendicular to the magnetic polar axis for intermediate magnetic obliquities, including those they obtained for σ Ori E.

The spectroscopic anomalies of σ Ori E (HD 37479, B2 Vp; Lesh 1968) were first noticed by Berger (1956) and discussed further by Osmer & Peterson (1972). This star is the prototype and most studied of the helium-strong subclass of Bp stars. Walborn (1974) discovered Hα emissions in this star's spectrum that varied on a timescale of hours. This variability was subsequently established to be associated with the rotation of a frozen-in disk, as described above. Hesser et al. (1977) determined a

⋆ Based on observations obtained at the the Dominion Astrophysical Observatory, Herzberg Institute of Astrophysics, National Research Council of Canada.

⋆⋆ *Present address*: Space Telescope Science Institute, 3700 San Martin Dr., Baltimore, MD 21218.

Article published by EDP Sciences and available at http://www.aanda.org or http://dx.doi.org/10.1051/0004-6361:20078196

period of 1.19081 days based on several nights of photometric observations distributed over a few years. Subsequently, various studies (Landstreet & Borra 1978; Bohlender et al. 1987) determined that the magnetic variations (suggestive of an approximately dipolar field with polar field strength $B_p \approx 10$ kG) are consistent with the photometric period. Various periods over the range 1.19081–1.19084 days have since been determined by several authors from analyses of variations of photospheric and circumstellar Hα line emissions (Hesser et al. 1977; Reiners et al. 2000, hereafter R00; Townsend et al. 2005, hereafter TOG05).

Groote & Hunger (1976, 1977 hereafter GH76 and GH77) discussed the variations of high-level Balmer lines based on only photographic spectra. The GH76 data indicated that two disk occultations of the star, about 0.4 cycles apart, cause high-level Balmer line absorptions visible at these times. At the same times, the intervening disk material absorbs flux just shortward of the Balmer edge. Although the analysis of line absorptions do not generally allow us to infer the extent and total volume of such a corotating structure, these absorptions do yield considerable information about its three dimensional geometrical character. Smith & Groote (2001, hereafter SG01) combined strength and shape information of many ultraviolet metallic lines obtained by the *International Ultraviolet Explorer* around the rotation cycle to exploit this potential. Their study provides some of the first estimates of the physical parameters of the disk gas, including disk temperature, column density, and areal coverage of the star. The limitations of this study were the low signal-to-noise ratio and the paucity of phase sampling of the archival database. What has been needed is a study that includes complete rotational phase coverage of absorption lines sensitive to electron density. To respond to this need, we have obtained complete phase coverage of the hydrogen lines from H9 (Hζ) to the Balmer edge over the entire rotation period of σ Ori E. Such datasets have the potential to better elucidate areal coverage and density structure of the absorbing disk segments than has previously been possible.

2. Observations and modeling methodology

2.1. Observations

In an attempt to search for variations in high-level Balmer lines from the variable occultation of σ Ori E by its circumstellar disk, we obtained 114 spectra with the 1.85 m Plaskett telescope of the Dominion Astrophysical Observatory (DAO) on seven nights between 2007 January 25 and February 28. We used the f/5 Cassegrain spectrograph with an 1800 l/mm grating blazed at 5000 Å and the SITe-2 CCD. Despite the sometimes mediocre seeing at the DAO, we used a narrow 1 arcsec slit rather than an available image slicer in order to maximize the resolution and to permit background sky subtraction. We note, however, that observing conditions and seeing were very good on each of our observing nights. Exposure times were 15 min and to minimize the effects of any possible flexure in the spectrograph Fe/Ar comparison arc reference spectra were obtained approximately every hour. The data were processed in a standard fashion with IRAF[1]. The resulting spectra have a dispersion of 10 Å mm^{-1}, a resolution of about 16 400, and cover the wavelength region $\lambda\lambda$3645−3863. Typical signal-to-noise ratios, as measured in a flat region of the spectrum near λ3850, are about 150 per pixel. Table 1 provides a journal of observation numbers (the DAO 1.8-m odometer numbers for 2007 spectra), observing times expressed as Heliocentric Julian Day (HJD) and rotational phases.

[1] IRAF is distributed by the National Optical Astronomy Observatory, which is operated by the Association of Universities for Research in Astronomy (AURA), Inc., under cooperative agreement with the National Science Foundation.

2.2. Spectral synthesis computations

To perform the analysis of the high-level Balmer line and continuum spectra, we utilized a pair of programs written by Hubeny and Lanz with both LTE (Kurucz 1993) and non-LTE models in the BSTAR2006 series (Lanz & Hubeny 2007). The first of these, *synspec,* is a photospheric line synthesis program that computes the line and continuum photospheric spectrum of a star (Hubeny et al. 1994). We also made use of *synspec*'s capability of convolving the photospheric lines with functions approximating the instrumental and rotational broadening. We computed the synthetic spectra in steps of 0.01 Å.

The goal of our analysis was to compute effects of the high-level Balmer lines and Balmer continuum due to the intervening disk during each of the two occultation events that occur during σ Ori E's rotation cycle. Since it is already known from the SG01 study that the disk is cooler than the photosphere, these effects will only include absorptions. To simulate these absorptions we used the radiative transfer program *circus* (Hubeny & Heap 1996). This program computes strengths of absorption or emission components of lines in a circumstellar medium from user-input quantities such as disk temperature, column density, areal coverage factor (the portion of the disk that passes in front of the star), and microturbulent velocity. *Circus* combines this contribution with the *synspec*-computed spectrum of the photosphere. In the solution of the radiative transfer in its "LTE mode", *circus* calculates the line absorption reemission along a line of sight according to an input disk temperature, $T_{\rm disk}$. The physical rationale for choosing this convenient mode is that the formation of the Balmer line flux in the disk is believed to be due to recombination, and the atomic levels of the high-level lines and continuum may be plausibly assumed to be close to equilibrium with the gas kinetic temperature. As a reference point, we first considered temperatures near 12 750 K, the value SG01 found for $T_{\rm disk}$ from an analysis of low-excitation UV metallic lines. As detailed below, at one point in our analysis we also used the *circus* "scattering" (no reemission) approximation to gauge the effects of non-LTE in the disk formation of Balmer line cores. In addition, we point out that absorptions from the corotating disk are formed at these same Doppler velocity as for the background star, i.e., no differential velocities were imposed along the line of sight. Although *circus* is capable of computing the spectrum for as many as three circumstellar cloud components, our initial assessment of the equivalent width (EW) variations suggested that the absorbing disk segments have a complicated density stratification perpendicular to the disk plane. Since these details can not yet be explained by ab initio models, it was sufficient to describe the absorptions in terms of a single-component cloud model in our *circus* analysis.

3. Description of disk-induced absorptions

3.1. Equivalent width variations over the cycle

To survey the absorptions of the high-level Balmer series in our spectra, we chose the members H9, H12, and H14 for EW measurement. To these members we added the He λ3819 line, as it showed important differences with respect to the Balmer lines. We selected the Balmer H9 line for study because of its

Table 1. σ Ori E observing log including DAO 1.8-m spectrograph 2007 odometer numbers. Heliocentric Julian Dates – 2 450 000.0 and rotation phases are given in Cols. 2 and 3. The phases are derived using a formal period of 1.190 841 days and the 1976 zeropoint of HJD 2 442 778.819 used by Hesser et al. (1977) – see text.

Obsn. #	HJD	ϕ	Obsn. #	HJD	ϕ	Obsn. #	HJD	ϕ	Obsn. #	HJD	ϕ
069	4125.724	0.480	373	4130.696	0.655	453	4131.774	0.561	637	4133.674	0.156
072	4125.748	0.500	375	4130.709	0.666	454	4131.785	0.569	638	4133.684	0.165
073	4125.758	0.509	376	4130.720	0.675	456	4131.796	0.579	639	4133.695	0.174
074	4125.769	0.517	377	4130.730	0.684	457	4131.807	0.588	641	4133.707	0.184
076	4125.783	0.529	378	4130.741	0.693	508	4132.622	0.272	642	4133.718	0.192
077	4125.794	0.538	380	4130.752	0.702	509	4132.632	0.281	643	4133.728	0.201
078	4125.804	0.547	381	4130.763	0.711	510	4132.643	0.290	644	4133.738	0.210
079	4125.814	0.556	382	4130.773	0.720	511	4132.653	0.298	646	4133.750	0.220
298	4129.672	0.795	383	4130.784	0.729	513	4132.665	0.308	647	4133.761	0.229
299	4129.682	0.804	385	4130.796	0.739	514	4132.675	0.317	648	4133.771	0.238
300	4129.693	0.813	386	4130.807	0.748	515	4132.686	0.326	649	4133.782	0.246
301	4129.703	0.822	387	4130.817	0.757	516	4132.696	0.335	651	4133.794	0.256
303	4129.715	0.831	388	4130.828	0.766	518	4132.708	0.345	652	4133.804	0.265
304	4129.726	0.840	389	4130.840	0.776	519	4132.719	0.354	653	4133.814	0.274
305	4129.736	0.849	390	4130.850	0.784	520	4132.729	0.362	654	4133.825	0.283
306	4129.747	0.858	436	4131.623	0.434	521	4132.740	0.371	795	4159.640	0.960
308	4129.758	0.868	437	4131.634	0.443	523	4132.751	0.381	796	4159.651	0.970
309	4129.769	0.877	438	4131.644	0.451	524	4132.762	0.390	797	4159.662	0.979
310	4129.779	0.885	439	4131.655	0.460	525	4132.772	0.399	798	4159.672	0.988
311	4129.790	0.894	441	4131.667	0.470	526	4132.783	0.407	800	4159.687	0.000
313	4129.802	0.905	442	4131.677	0.479	528	4132.794	0.417	801	4159.697	0.009
314	4129.813	0.914	443	4131.688	0.488	529	4132.805	0.426	802	4159.708	0.018
315	4129.823	0.922	444	4131.698	0.497	530	4132.815	0.435	803	4159.718	0.026
316	4129.834	0.931	446	4131.710	0.507	531	4132.826	0.443	805	4159.731	0.037
317	4129.844	0.940	447	4131.720	0.515	631	4133.620	0.111	806	4159.741	0.045
319	4129.856	0.950	448	4131.731	0.524	632	4133.631	0.120	807	4159.751	0.054
370	4130.665	0.629	449	4131.741	0.533	633	4133.641	0.128	808	4159.762	0.063
371	4130.675	0.638	451	4131.753	0.543	634	4133.652	0.137			
372	4130.686	0.647	452	4131.764	0.552	636	4133.664	0.147			

proximity to the He I line and therefore the convenience of exploiting a nearly common local continuum level that would allow reliable measurements of line core and wing variations. The H12 and H14 lines were chosen arbitrarily because they measure effects of yet higher atomic levels (such as diminished line opacity), and they are largely redundant to one another. This advantage allows one to check the consistency of the EW variations.

For our line analysis we first rectified each spectrum by identifying maximum fluxes along the spectrum and fitting consistent orthogonal polynomials through these points using the *IRAF* task *continuum*. "Raw" EWs were measured from fluxes within ±2.5 Å of the line centers; for H14 this window was relaxed to ±2.4 Å. These windows were chosen because they delimit the absorption from the disk occultation. For the initial measures these core depths were referenced to a pair of quasi-continuum points intermediate between the line to be measured and the nearest hydrogen and helium lines. One of these points falls between the closely occurring He I λ3819 and H9 lines. This circumstance allowed us to check for residual errors in local continuum placement. Such errors would produce similarly low or high EW measures in both these lines at the same phase, rather than the opposing variations in these two lines caused by deviations from the mean of the surface He/H value as the star rotates. Because our analysis is based on absorption *excesses* of the line cores, our measurements can be tied directly to the computed absorptions in our disk models.

We noticed that our raw EWs were significantly affected by an approximately single-waved variation in the line wings that is well correlated with the variation of the He I line measures and hence instantaneous integrated He/H abundances measured by R00. We corrected for this effect by first measuring the variable fluxes in their wings at windows between ±2.5 Å and ±5 Å from line center. These fluxes are not affected by the disk. The wing EW components of the H and He I lines vary in perfect anti-correlation. We chose an arbitrary reference phase of $\phi = 0.35$, which corresponds to the middle of an extended low plateau of the strength of helium lines (R00), signifying a near-normal He/H abundance for the region of the star visible during this phase. We then corrected the core EWs using an empirical relation derived from the slowly varying wing and core variations for the H9 and He I lines throughout the cycle (excepting the brief occultation maxima discussed below). Noticing that this correction resulted in an equality of the two H9 line EW minima, we adopted similar relations for the H12 and H14 line EWs that forced equal EWs in their minima as well. Figure 1 exhibits the corrected variations through the rotation cycle for these four lines. Different symbols are used for different nights' observations to best exhibit the (generally negligible) night to night differences in our measurements at thoses phases observed on multiple nights.

The panels exhibit several interesting details in the Balmer and He I line absorption curves of σ Ori E. First, the EW curves exhibit two maxima at $\phi \approx 0.0$ and 0.4. Distinct minima are also apparent at $\phi = 0.85{-}0.90$ and 0.55. We will refer to these as the primary and secondary absorption maxima and minima, respectively. The exception to this statement is that the primary maximum is absent in the He I line curve and the secondary

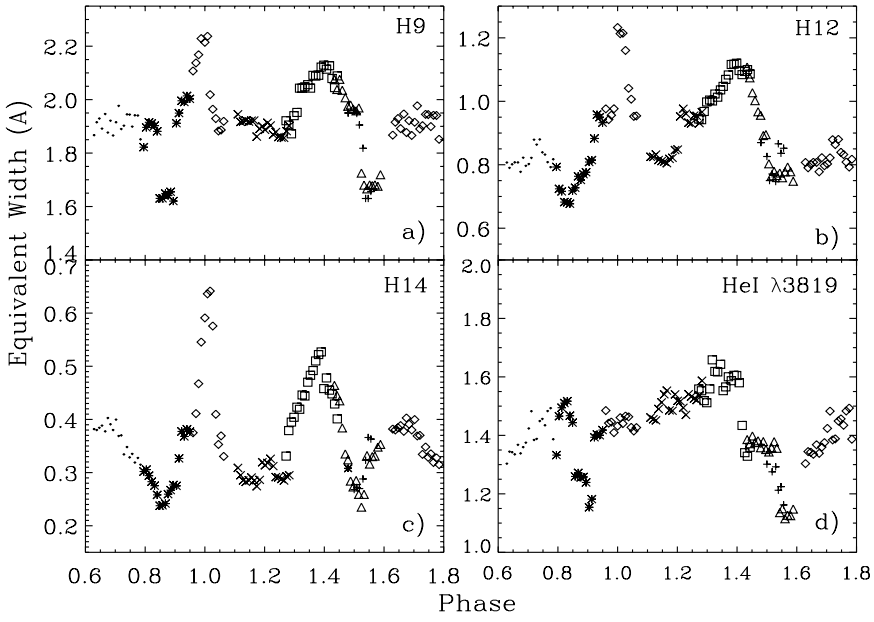

Fig. 1. Equivalent width curves plotted as a function of rotational phase using the ephemeris in Table 1. The EWs are defined from local "continuum" points located between the hydrogen lins. Represented are panel **a)** H9, panel **b)** H12, panel **c)** H14, and panel **d)** He I λ3819 lines observed during 2007. Symbols are: pluses (25 Jan.), stars (29 Jan.), diamonds and dots repeated a cycle earlier (30 Jan.), triangles (31 Jan.), squares (1 Feb.), crosses (2 Feb.), and diamonds (28 Feb.; at $\phi = 0$, corresponding to observation #800 for all lines).

maximum is only weakly present. The existence of the brief minima was surprising because they have not been noticed in previous EW studies in the UV and optical (e.g., R00, SG01). As our *circus* analysis will also show, all of the lines are optically thick, but the H14 line is significantly less thick than H9. Additionally, one notices differences in the approach of these curves to their maxima and minima. The edges of some of these plateaus are sharp, and this is likely to be a manifestation of the line opacities changing from optically thin to thick regimes.

The primary maximum differs in morphology from the secondary feature, being more short-lived and triangular. Observation #800 coincides with the maximum EW for all the H lines. Following, Hesser et al. (1977), we assign $\phi = 0.0$, defining the line flux minimum with the midpoint of this observation #800, HJD 2 454 159.687, as the epoch-defining flux minimum. For completeness, we note that if one adopts Hesser et al.'s 1976 epoch of HJD 2 442 778.819, uses the cycle counts of R00, and assumes that the period has been constant over this 10 000 cycle interval, a period of 1.190841 days would result. However, we hesitate to claim this formally as the star's true period (or to assign error bars) because the apparent phase difference in photometric minimum and line strength maximum of 0.02 cycles suggests that caution should be exercised in combining hetergeneous data types – that is our $\phi = 0$ corresponds to 0.02 for the Stromgren filter *u* minimum phase of Hesser et al., according to the GH77 phases. If correct, this would modify the value of the period to 1.190839 days. We also point out that the most current value of a wholly photometrically derived period, 1.190832 days (Townsend 2007), is only 3σ from the above value, according to the errors we would perhaps simplistically assign to our own measurements.

In addition to the maxima and minima, minor brief changes in the absorption take place, such as that occurring at $\phi = 0.80$ in the strong lines H9 and He I λ3819. More conspicuously, the flat plateaus at $\phi = 0.7-0.8$ in the EW curves of these lines are not shared in the weaker H12 and H14 curves, suggesting a thinning of absorbing circumstellar material that is first betrayed in the least optically thick lines. Brief minor absorption bumps can be seen in these curves near $\phi = 0.20$ and 0.93. Altogether, there is substantial evidence for the existence of static, high-latitude circumstellar matter. The fact that these absorptions are present to some extent in He I argues as well that this matter is heated more than, for example, the disk segment responsible for the primary absorption. The excitation of this matter is still influenced by a largely undiluted UV radiation field from the nearby star.

We end this section by discussing whether the EW variations in Fig. 1 could be due to the passage across the disk of surface inhomogeneities, which could influence the line strengths either through changing the number of absorbers in the line or indirectly through their influence on the structure of the photosphere. To address this hypothetical problem, we stress that the wings of these lines *do* respond to such changes consistently with EW variations of the He I lines, including the λ4713 line depicted by R00 (e.g. during the phase interval $\phi = 0.65-0.80$) and do not deviate from the anti-correlation established from this interval at intervals when the H I and HeI line cores undergo sudden changes. Second, the occultation maxima found in Fig. 1 develop in very short intervals, contrary to the slower variations of at least 0.15 cycles for which the He I and metal line strengths evolve (R00; Groote 2007).

A third reason for doubting that inhomogeneities influence our line wing measurement derives from results using specialized model atmospheres results appropriate to Bp stars with He and metallic patches. In particular, Krtička et al. (2007) have studied the effects of chemical inhomogeneities on the surface of the B2p star HD 37776, another B2p star with a very strong magnetic field. Both the abundance variations across the surface and the magnetic field strength are at least 10 times greater than those in σ Ori E. These authors find that photometric variations of this star are likely due to the effects of bound-free absorption edges produced by abundance patches of elements like silicon (the iron abundance is depleted). They show that the temperatures of superficial regions of the photosphere should be elevated by this added opacity. Because this is the general region where most line cores and bound-free edges are formed, the effect is to cause a weakening of the line cores arising from "passive" species, in this case helium and hydrogen atoms. The metals and helium variations are anti-correlated because for both σ Ori E and HD 37776 the metals are less depleted in belts distributed on the magnetic equator. Thus, the passages of patchy regions

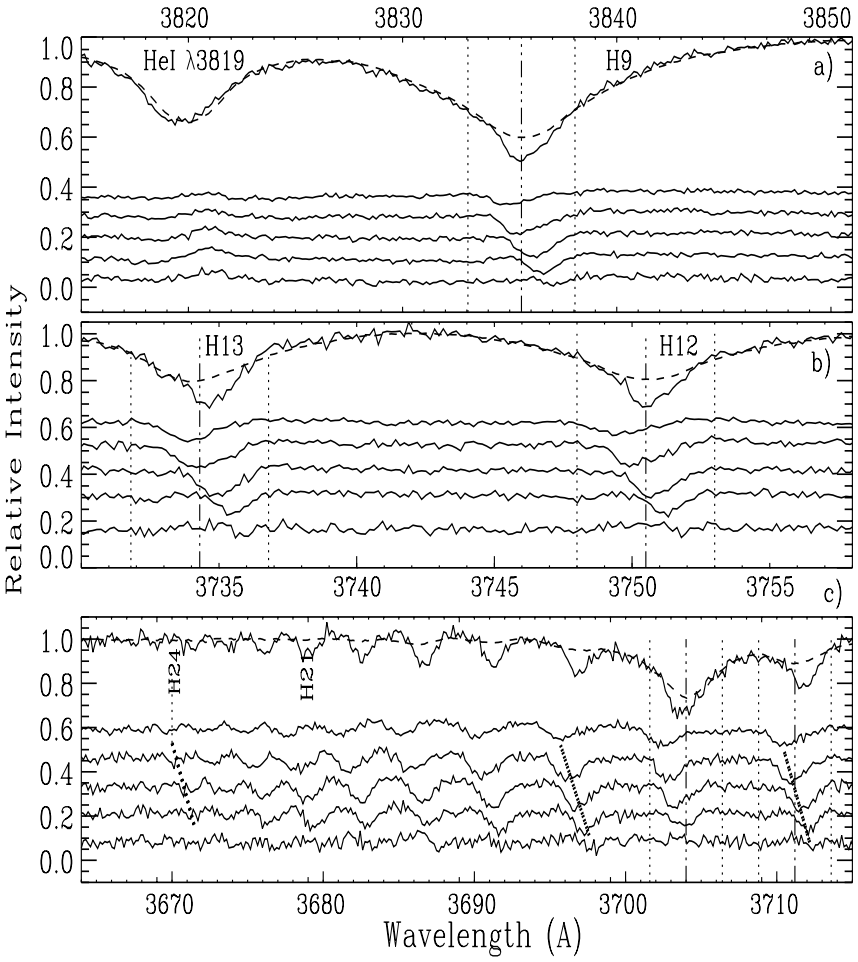

Fig. 2. Montage of mean and differences profiles through the primary occultation event. Bottom spectra depict difference profiles with time (downward); top spectra are the mean spectrum of the non-absorption times at ϕ = 0.85−0.90 and the observation #802 (ϕ = 0.18) for which the central absorption lobe crosses the mean profile. Panels **a)**, **b)**, and **c)** represent the spectral region around H9 and λ3819, H13 and H14, and H15−H24. Sloped dotted lines trace the migration of subfeatures in three lines with time. The difference spectra refer to observations #798 & 800, 801–802, 803, 805–806, and 807–808. These correspond to approximate phases of 0.99, 0.01, 0.03, 0.04, and 0.06, respectively.

of the star's surface, irrespective of an intervening disk, produce continuum light variations. Returning again to our spectroscopic data for σ Ori E, and utilizing the Krtička et al. simulations, the cores of hydrogen and helium lines should weaken during these phases according to our hypothesis – yet they do not. We note in particular that this fact shows that the slight enhancement of the He I λ3819 line in Fig. 1 cannot be attributed to surface inhomogeneities on the star.

3.2. Line profile variations

To represent the line profile variations of the two occultations, we compared individual or pairs of line profiles differenced against average profiles of the two minima. Specifically, for the first stretch of absorption minimum centered at ϕ = 0.87 the mean was computed from observations #305−311, and for the second minimum (ϕ = 0.55) from observations #448−457. Figures 2 and 3 exhibit, at the bottom of each panel, the migration of absorption lobes across the profile for He I and H9, H12 and H13 line, and H15 and higher for both occultation events. At the top of each panel we depict the rectified unabsorbed mean spectrum and an example of one of the observations during the occultation. Close inspection of the difference spectra during the second occultation discloses the passage of two lobes across the profile. In our depiction the two lobes can be discerned in Fig. 3 by the flat-bottomed difference profiles of observations #513–515 (ϕ = 0.31–0.33), followed by a second flat-bottom in the #523–524 (ϕ = 0.38–0.39) profiles. The second lobe in the second occultation can be parameterized by a ∼50 km s^{-1} Gaussian and is deeper than the first one. The first lobe of this occultation, as well as the lobe of the first occultation, are slightly narrower and can be fit with a ∼40 km s^{-1} Gaussian.

From Fig. 2 we estimate that the midpoint of the first occultation, as judged from the transit across the profile of the centroid of the excess absorption lobe, occurs for observation #802 (ϕ = 0.018), or ≈0.02 cycles later than the observation responsible for the maximum hydrogen EWs in Fig. 1. Our error estimate given above was obtained from the 0.02 cycle difference between the light minima and line profile passage events found by GH76.

The difference between times of passage of the absorption line in the profile and EW maximum for the whole line carries over to the second occultation. From Fig. 3 because of the finite signal to noise, the breadth and unequal depths of the features we cannot establish a reliable phase for the mid-point of the occultation. Our best estimate is at the beginning of observation #524 (ϕ = 0.390), which would be some 0.37 cycles after the central lobe passage in the primary event and identified with observation #802 (ϕ = 0.018). Thus, whereas there is a separation of 0.40 cycles between the EW maxima, the separation between the lobe passage events is somewhat smaller. Similar structure can be discerned in the semi-resolved double lobes, centered at $\phi \approx$ 0.35 and 0.42 of the secondary occultation in the light curves of Hesser et al. (1977) and Oksala & Townsend (2007). Perhaps related to the complicated shape of the secondary EW maximum is the fact that our best estimate of the separation between this and the primary occultation, 0.40 cycles, is about 0.02 cycles smaller than the value determined from

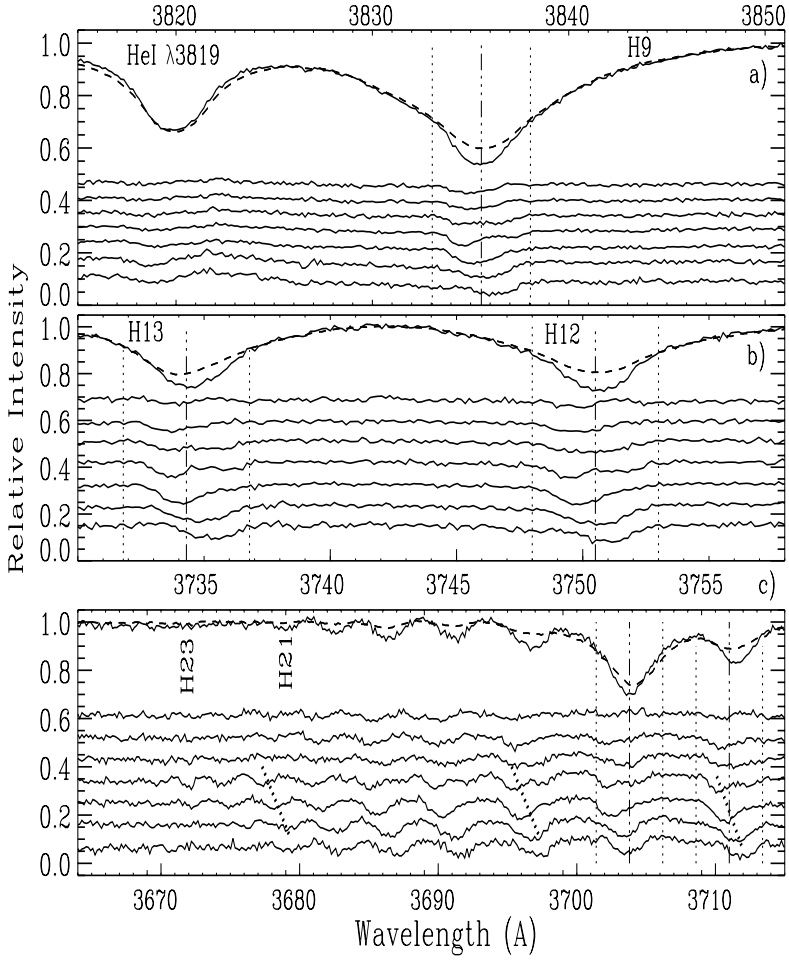

Fig. 3. Montage of mean and differences profiles through the secondary occultation event. Pairs of difference spectra with time (downward) are depicted at bottom. Spectra at the top are the mean spectrum of the non-absorption times at $\phi \approx 0.55$ and the observation #524 for which the central absorption lobe crosses the mean profile. Difference spectra refer to observations #509−510, 513−515, 516−518, 519−520, 521, 523−524, and 525−526. These correspond to approximate phases of .29, .32, .34, .36, .37, and .38, and .40, respectively.

the Hesser et al. (1977) and the nearly contemporaneous Oksala & Townsend (2007) light curves. It is not clear to us whether this minor discrepancy has any consequences on the details of the disk model. The most conservative assumption is that the opacity (column density) of the disk is unequal at opposing positions on either side of the central plane. As already suggested from resonance line data (GH97; SG01), a disk "warping" could explain in principle both the appearance of a minor lobe within the secondary occultation event as well as an *apparent* unequal fall off in column density at small and opposite phases from the central maximum absorption. This circumstance would likely affect optically thin (photometric) and thick (Balmer line) measurements differently.

In the curves of the primary and secondary occultations (Figs. 2c and 3c) the Balmer line series can be discerned out to H24 and H23, respectively. (We note that differences formed against the mean of all spectra except those in the two occultations have a higher signal quality and bring out these limiting lines more clearly.) We will return to these limiting line members in our later discussion of electron densities in Sect. 4. In the lower panels of Figs. 2 and 3 we have also indicated the acceleration of the absorption lobes through the profile. A cross-correlation analysis of the shifts of the line with respect to a fiducial spectrum discloses that the average acceleration of these features is 72 km s^{-1} h^{-1} and 50 km s^{-1} h^{-1} for the primary and secondary occultations, respectively. The larger accelerations of the features occurring during the primary occultation (assuming the disk is rigidly rotating) indicate that it lies further from the star than the disk segment producing the secondary occultation. As pointed out earlier, the absence of the He I line absorption during the primary occultation is likewise consistent with this segment lying further from the star.

3.2.1. Balmer line and continuum absorptions

In preparation for a *circus* analysis of the physical parameters of the absorbing disk segments, we have computed ratioed spectra of the means of the raw (unrectified) spectra. These exhibit the largest absorptions during the two occultations (observation #800 for the primary, and observations #516–524 ($\phi \approx 0.36$) for the secondary) with respect to the absorption minima spectra occurring at nearby phases (observations #305−311 and observations #448−457, or $\phi \approx 0.86$ and 0.56, respectively). These spectra and the ratios are depicted in the two panels of Fig. 4. These panels show the clear absorptions in both the lines and the effective Balmer continuum, which starts at λ3690−3700. The ratios $F(\lambda 3650)/F(>\lambda 3700)$ for the occultations come to about 0.845 and 0.925. We will use *circus* to reproduce these ratios in the next section.

It is worth pointing out that the Balmer continuum absorption in these particular pairs of specra are unlikely to be contaminated significantly by the effect of telluric UV absorption through different air masses. For example, in the case of the primary occultation, the observation was obtained at an hour angle (HA) of 0:49, as compared to the nearly equivalent value of a mean HA of 0:47 for the observations comprising the minimum

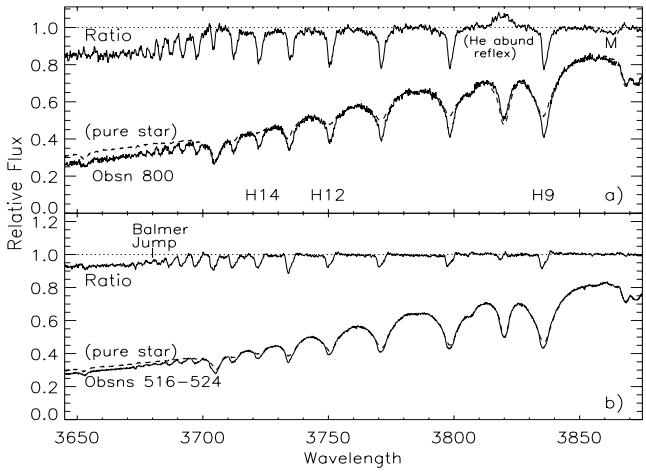

Fig. 4. The spectrum exhibiting the maximum absorption during central occultation and the mean spectrum representing no disk absorption referenced in previous figures. The ratio of these spectra are depicted at the top. Panels **a)** and **b)** represent the primary and secondary occultations, respectively. In **a)**, by "M" we denote metallic line features used in the text to set a rough disk temperature and also the weakened helium line (shown as apparent "emission") due to chemical inhomogeneities. The Balmer jump is represented by the lower flux shortward of about λ3690.

spectrum. The respective HAs for the secondary event are likewise practically identical: 0:33 and 0:36. These differences are less than the exposure times of the spectra (15 min).

The hydrogen line absorptions show no noticeable radial velocity shift ($<\pm5$ km s^{-1}), and they are confined entirely within ±2.5 Å of the line cores. One anomaly in the primary occultation spectrum (Fig. 4a) is that the He I λ3819 actually appears *weaker* during the occultation. This effect reflects the passage of a He-rich spot at phases $\phi = 0.8$–0.9 (R00), from which spectra used to compute the *hydrogen* line minimum were taken.

4. Determination of disk parameters

The primary estimates we are able to make for the disk segments causing the hydrogenic absorptions come from analysis with the *synspec* and *circus* models. We adopted a solar H/He abundance in our disk models. However, since these are unlikely to be strictly correct (assuming the He/H abundance in the disk sustantially reflects the values for the material at both magnetic poles), the column densities we derive should be understood to refer to hydrogen atoms.

4.1. Rotational and magnetic axes inclinations

We have discussed the likelihood already from the discussion of EW and line profiles that a pair of disk segments residing near the intersections of the rotational and magnetic equators occult different regions of the star at times separated by approximately one-half of the rotation period.

Our disk analysis begins with an estimate of the stellar properties. We used Kurucz (1993) models with parameters $T_{\rm eff}$ = 23 000 K and $\log g = 4$ (e.g., Smith & Groote 2001). We computed the photospheric line profiles with a rotational velocity of 150 km s^{-1}. The foregoing geometric properties of the disk are not sensitive to these estimates.

The geometric constraints begin with a determination of the inclination angle i of σ Ori E's rotational axis as well as the angle between the rotational and magnetic axes – the so-called magnetic obliquity, β. Traditionally the former comes from comparing the star's projected rotational velocity with its radius as inferred from its position on a stellar evolutionary track. Estimates in the literature range from $i \approx 90°$ (Bohlender et al. 1987; Short & Bolton 1994; TOG05), to $i \approx 39°$ (R00). The latter value is based on an uncertain distance estimate. From detailed fitting of the light curve of the star to their Rigidly Rotating Magnetosphere (RRM) model, TOG05 found that $\beta + i \approx 130°$. They adopted $i \approx 75°$ and $\beta \approx 55°$. The intermediate value of β is based largely on the unequal spacings (0.4, 0.6 cycles) of the light minima of the light curve, which implies that the center of the stellar magnetic field is displaced 0.3 R_* perpendicular to both the rotational and magnetic axis and is also displaced 0.05 R_* along the magnetic axis. We note also that Groote (2003) gives $\beta = 67°$. However, this value is based on an analysis of the distribution of He/H on the surface. In particular, it is likely that the centroid of the He-rich patch is somewhat displaced from one of the two magnetic poles (e.g., Groote & Hunger 1997). An additional set of constraints can be placed on these angles from the shapes of the equivalent profiles of the two maxima. As already mentioned, the primary maximum in Fig. 1 has a triangular shape, and the two legs of this triangle have unequal durations. This occultation appears to be the one for which the segment passes most closely to the projected center of the star in the observer's line of sight. At $\phi = 0.4$ the opposing segment occults only the lowermost limb of the star during mid-passage. We will now investigate the shapes and intensities of the occultation profiles.

We have designed and discussed a disk occultation tool to quantify the absorption of light and equivalent width curves from an optically thick disk or, alternatively, from a thick disk surrounded by a translucent periphery at greater distances from the magnetic plane (see discussion and Figs. 6, 7 in Smith et al. 2006). We found that a triangular shaped occultation profile can be reproduced if the disk has a limited radial extent (i.e., it is ring-like) and/or its height perpendicular to the magnetic plane, is small. Another signature of a ring-like structure is if the ingress/egress edges of the occultation event are sharp. This can happen only if the disk is separated from the star.

Additional considerations in evaluating the disk geometry in our model are first, that the ratio of secondary to primary line and continuum absorptions is 1.3−1.4. We will use this range as a starting guess for the ratio of the stellar areas eclipsed by the disk segments. The amounts of the absorptions in the *circus* computations discussed below will also translate to the individual occultation areas. This leads to a secondary constraint that the angles i and β must be near 90° and not much larger than 55°, respectively. Otherwise, the measured Balmer continuum absorption cannot be attained by an occultation that is too weak when the disk crosses the "lower" limb of the star, as seen from our vantage point. Finally, the fact that there is just a hint of an M-like reversion in the secondary occultation profile limits the value of i to at least than 80° ± 5°. (However, if the two peaks result from disk warping this argument is questionable.) With the constraints we imposed above as well as TO05's arguments, this fixes the β value as near 55° ± 5°. These values are in reasonable agreement with estimates based on different criteria by other authors.

For completeness, we find that for $i \geq 80°$, a period of 1.19 days, and its $v \sin i$ of 140–162 km s^{-1} (e.g., Bolton et al. 1986; R00), the mean radius of σ Ori E comes to 3.4–3.9 $R_\odot$. As

Table 2. Derived absorbing disk parameters (assuming $i = 80°, \beta = 55°$).

Primary Occultation:		Secondary Occultation:	
Outer radius	$5-6 \pm 0.5\ R_*$	Outer radius (2 solutions)	$2-4\ R_*$
Radial thickness	$2.5-3\ R_*$	Radial thickness	$0.25-2.8\ R_*$
Height	$0.3 \pm 0.07\ R_*$	Height	$0.45 \pm 0.10\ R_*$
Temperature	10 500 K ±1000 K	Temperature	12 000 K ±1000 K
N_e	$1 \pm 0.5 \times 10^{12}$ cm^{-3}	N_e	$1 \pm 0.5 \times 10^{12}$ cm^{-3}
Column density	$1 \pm 0.5 \times 10^{24}$ cm^{-2}	Column density	$1 \pm 0.5 \times 10^{24}$ cm^{-2}
Areal coverage	0.45 ± 0.10	Areal coverage	0.31 ± 0.10

is by now well known (e.g., Hunger et al. 1989), these radius estimates seem low for a B2 main sequence star, but we can offer no solution to this apparent dilemma.

4.2. Disk dimensions

The dimensions of the disk segment responsible for the primary occultation can also be inferred by appealing to Hα emission studies, which provide estimates of $5-6.4\,R_*$ for the outer disk dimension (Groote & Hunger 1982; Short & Bolton 1994; TO05), the accelerations and durations of the absorption lobes in Figs. 2 and 3, and the areal coverage arguments of the previous section. Our simulations also show that for the primary occultaion the outer radius must be at least $4\,R_*$ in order for the disk to have a finite thickness in the radial extent. Table 2 gives the dimensions of the absorbing disk segments in units of stellar radii as well as the mean densities and temperatures of our solutions. The radial thickness refers to the quantity $R_{\rm outer} - R_{\rm inner}$. We note that the derived radius is consistent with that given from the durations of the lobe apparitions found in Figs. 2 and 3. The errors for these parameters are about ±20%. For the primary absorption the results pertain to the rise time phase for the first half of the event, which lasts 0.04 cycles. The shorter span for the decline (0.03 cycles) of the second half can best be simulated by decreasing the semiheight from $0.3\ R_*$ to $0.2\ R_*$. These parameters also preserve the triangular shape of this primary occultation profile.

The challenge for deriving the dimensions for the disk segment causing the secondary absorption maximum is that they should be large enough to ensure enough areal coverage of the star and to produce the observed absorption in the Balmer lines and the Balmer jump. In general, lower values of β and $R_{\rm outer}$ and larger h values insure this. A value of $R_{\rm inner} > 2\ R_*$ is impossible to reconcile with the observed amplitude and shape of the occultation profile with phase in our models with the assumed β and i angles. However, if one adopts the view that the extended lifetime of the occultation is due to seeing two different radial zones of the same segment along a line of sight (i.e., the disk is warped), one can relax the distance $R_{\rm outer}$ up to $4\ R_*$ (but no higher). Since this constraint is consistent with the ratio of the radii suggested by the two acceleration rates determined in Sect. 3.2, we cannot rule this out. We have added this possibility in Table 2 by showing the admissible ranges of the inner and outer radii. parameter to the assumption of disk warping, i.e. $2\ R_* \le R_{\rm outer}$ We also point out that in the warping interpretation, $R_{\rm inner}$ can move in to $1.2\ R_*$, so the disk extends *almost* to the star's surface.

According to our picture, at the middle of the first occultation at $\phi = 0$ the whole of the disk segment is silhouetted against the star. For this portion of the disk we may estimate the mass from the dimensions of the segment (area and column density) and its density. This gives a mass of about $5 \times 10^{-11}\ M_\odot$. If we take half the mass loss rate as the rate of resupply of this hemispheric disk segment ($1.2 \times 10^{-9}\ M_\odot$ yr^{-1}; Krtička et al. 2006), the mass loss will replenish this disk segment in about 2 weeks. Because a small fraction of the wind emanating from close to the magnetic poles will avoid being focused into the disk and, further, because we may not see the full disk segment in azimuth around the hemisphere, the actual lifetime of the particles in the disk will be somewhat longer[2]. Note that the transit of a disk across the star lasts only $\lesssim 10^{-3}$ of this time. Therefore, leakage of disk particles either into the star or through its outer edge would produce a tapered absorption wing that is too small to be visible in our data.

We conclude this discussion by calling attention to the EW minima within the general model for the disk, which occurred on a total of three of the seven nights of our observing run on this star. One explanation for these minima is that a second translucent component exists layered over the more confined opaque disk. In this explanation, we would be looking through a light "haze" (with about 1% of the column density) through most viewing aspects. However, little if any tail is observed in the curves of Fig. 1. (This fact underscores our finding above that the density contrast of the disk proper relative to circumstellar matter at moderate or high magnetic latitudes is rather high.) A second possible way to explain the EW minima is that they are "reflexes" of small incipient emissions that may still be detectable in the high level lines. Indeed, FEROS observations of the Hα line at these phases (Groote 2007) exhibit strong emissions and an elevation of the line core at these phases. In this event there would be no need of a pervasive low-absorption component.

4.3. Thermodynamic parameters of the disk segments

The Balmer absorption spectra of Fig. 4 provide sufficient information to estimate the temperature, electron density and column density of the intervening disk segments. To make these estimates, we must assess the importance of errors in various factors used in these calculations. First, and importantly, the assumed areal coverages depend strongly on the geometrical angles derived above. Despite our agreement with earlier authors, errors in our estimates of these parameters propagate to the areas in complex ways and should be considered the largest source of our uncertainty. Second, it turns out that the disk microturbulence, ξ, is *not* an important factor. We find almost identical solutions for fitting excess Balmer line and continuum absorptions for values of ξ in the range $0-20$ km s^{-1}. We have arbitrarily adopted a value $\xi = 10$ km s^{-1}. Third, we have used non-LTE model atmospheres computed from the BSTAR2006

[2] The fact that our column densities are averaged over the disk height will cause the total density and hence mass in our model to be underestimated. We may reasonably expect the longevity of particles in the disk to be a few months.

grid (Lanz & Hubeny 2007) and found that the photospheric Balmer jumps for LTE and non-LTE model atmospheres differ negligibly given the adopted $T_{\rm eff}$ for σ Ori E. This can be inferred also by examining Fig. 6 of Lanz & Hubeny. These authors find that changes in abundances have little effect on photospheric temperatures in the range $\tau_c = 0.01{-}0.003$, where much of the Balmer line cores is formed.

SG01 pointed out that the presence of certain low resolution line aggregates in the far-UV spectra suggest the presence of a cool component to the disk of σ Ori E having a temperature of about $12\,750\,{\rm K} \pm 750\,{\rm K}$[3]. In this study we discovered a weak but important diagnostic in the excess absorption spectrum of the secondary occultation (Fig. 4b), namely weak absorption blends at λ3760 and $\lambda\lambda$3855−60 arising primarily from transitions of once ionized light and iron-group metals. Our *circus* syntheses show that these lines appear for $T_{\rm disk} \leq 12\,000\,{\rm K}$ over disk column densities of interest.

Our primary modeling diagnostic for column density and areal coverage is the excess Balmer jump noted in Fig. 4. While potentially useful, the Balmer lines themselves were found to be enhanced primarily by non-LTE effects. Thus, whenever the excess absorption below $\approx\lambda$3647 could be fit, the disk Balmer line spectrum is far too strong. We will therefore confine ourselves to fitting the Balmer jump in the following discussion.

The electron density $N_{\rm e}$ of the disk medium can be determined by the presence of the highest-level Balmer lines in the occultation spectra (Fig. 4). One might first draw an analogy to the prominence of these lines in the spectra of B supergiants. For low density atmospheres, the lines are visible because the weak Stark wings cause less blending. This motivated us to inquire whether the Inglis-Teller (1939) criterion might apply in this instance. This condition gives as an estimator that the last visible line of an hydrogenic spectrum scales with the electron density as $N_{\rm e}^{-7.5}$. By comparing the highest visible Balmer lines in the spectra of early-BIa stars (e.g., Bagnulo et al. 2006) and appealing to model atmospheres for stars of these temperatures and gravities (e.g., Crowther & Lennon 2006), we found that the visibility of H24 and H23 in occultation spectra suggest $N_{\rm e}$ values of 1×10^{12} and 2×10^{12} cm^{-3}, respectively. However, this argument may not be precise as our spectra show that the strengthening of these lines occurs mainly in the line cores. Our modeling of these absorptions suggests that what is important in determining the visibility of the last Balmer line is the column density of high-level hydrogenic atoms producing the absorption. In particular, we find that through the Saha equation $N_{\rm e}$ is largely determined by fixing the column density at which the optical thickness of a high-level line is $\approx$1. For temperatures of interest (10 000–14 000 K) the density corresponding to the semi-visibility of H23–H24 is also $N_{\rm e} = 1 \times 10^{12}$ cm^{-2}. We found that the fitting of the Balmer continuum absorption is insensitive to the value of $N_{\rm e}$. Therefore, we adopt this density for both disk segments in our *circus* analysis of the disk segment parameters.

We adopted the densities from the above arguments to determine disk temperatures, column densities and fractional areal coverage factors needed from the Balmer jump found below λ3700 in Fig. 4. To add to these constraints, we also invoked the condition that the areal coverage ratio should be 1.3–1.4. However, we modified this by determining that a correction of about 10% for limb darkening (assuming a coefficient $\mu = 0.6$) is necessary to account for the transit of the disk segments across noncentral regions of the star. This consideration brings us to a ratio of 1.5 for the fractional areas. This condition is met by the entries in Table 2. Our models established quickly that the hydrogen column density should be near 1×10^{24} cm^{-2}. (However, the column lengths are not determined well enough to compare the radial distances of the two disk segments.) This condition derives from the broad opacity plateau at $\approx 1 \times 10^{-24}$ cm^{-2} in this wavelength region for the relevant temperatures. For substantially larger column densities the disk plasma becomes optically thick in the continuum, and the Balmer jump it forms begins to decrease. For smaller column densities one runs quickly into unrealistically large fractional areal coverages and the Balmer jump decreases owing to optical thinness of the Balmer continuum. Given these considerations, we believe that the column densities we found, which are coincidentally the same for the disk segments causing the two occultations, are accurate to within a factor of two. The fractional coverages we infer depend on this condition combined with the absorption ratio of 1.3−1.4 derived above from the two occultations.

Our estimated column density agrees well with the derived values of the electron density, 10^{12} cm^{-3}, the inferred radial extent of the disk ($2.5{-}3\,R_*$) for the segment causing the primary maximum and within a factor of two of that for the segment producing the secondary. Note that SG01 found a column density of 3×10^{23} cm^{-2} from the strengths of absorption of Fe aggregates and low excitation light-metal lines in the UV. When account is taken that SG01 assumed for simplicity a full occultation of the stellar disk, their column density is virtually the same as the value we derived from the assumed density and the values given in Table 2, $3{-}7 \times 10^{23}$ cm^{-2}. Our solution, assuming $\tau_{\rm continuum} \approx 2$ and disk homogeneity, likewise agrees perhaps fortuitously well with the peak value $\tau_{\rm continuum} \approx 1.6$ determined by TOG05 for the optical thickness viewed along the central magnetic plane. The latter determination was made for a decentered dipole that probably most accurately reflects the magnetic geometry.

Our homogeneous disk solution overlooks the evidence that the segment producing the secondary occultation occurs in two semi-resolved stages. As already mentioned, one interpretation of this is that the a warping occurs in the inner disk, as suggested by previous studies. In any case, this semi-resolved structure of the occultation is noticeable in light curves at several wavelengths as well. It may be that what observers identify as "warping" is in fact due to a departure from strict coplanarity predicted for extensive Bp disks for which the magnetic β obliquity has an intermediate value (TO05).

Returning to the Balmer lines, we were able to evaluate departures from LTE in the line source functions by comparing the column densities needed to fit the Balmer jump with those in the lines. As already stipulated, we assumed that the Balmer continuum flux is formed in the disk in near LTE. By comparing the column densities needed to fit the lines to the Balmer continua, we found for both occultations the same approximate ratios of source to Planck functions: $S/B = 0.006$ for H9 and $S/B = 0.1$ for H20.

Finally, the temperatures for the two disk segments are consistent with the radiative temperatures one would expect for radiatively excited matter close to the star. There is no evidence in these disk segments in particular for the heating responsible for the presence of the variable N V resonance lines (SG01).

[3] For studies of different lines and in a different wavelength regime, we estimate that the uncertainty of this mean disk temperature should be at least doubled. This uncertainty does not propagate to the more precise temperature *difference* quoted below for opposing disk segments.

5. Summary and conclusions

We have used high-level Balmer absorption data finely sampled around the rotation cycle to show that the distribution of plasma in the magnetosphere of σ Ori E is more complicated than previously believed. Most especially, the secondary occultation is comprised of two semi-resolved events. In addition, there seem to be at least two brief appearances of absorbing matter well beyond the disk plane. The disk plane is dominated by two segments which occult portions of the star some 0.4 cycles apart. We have no direct information from absorption profiles alone on the distribution of matter at other azimuths in the plane and so look forward to future analyses based on the Hα and/or Hβ emissions over the cycle.

The occulting disk segments are sections of a ring which occult the star as the frozen disk corotates around the star. The segment causing the primary occultation lies further from the star (between limits of $\approx$2.5 R_* and 6 R_*) than the opposing segment. There are at least three arguments that point to the disk segments lying at different orbital radii. First, gas in the segment causing the primary occultation has a lower temperatures (10 500 K, compared to 12 000 K). This can be inferred first from the lack of an enhanced He I feature and also from the absence of weak absorptions of metallic-line blends referred to in Sect. 4.3. Second, the acceleration of spectral migrating components across the line profile is higher for this segment. Third, our occultation analysis program indicates that one cannot reconcile the radii of the two segments even if one attributes the broad secondary absorption maximum as being due to viewing two occultations of a single warped disk segment.

Perpendicular to the magnetic disk, the semiheights of the two segments are some 0.3–0.45 R_*. It is important to stress that the disk of σ Ori E has a smaller semiheight than disks for other disk-harboring Bp stars that we have analyzed with similar modeling techniques (e.g., SG01; Smith et al. 2006). It is tempting to speculate that a disk should be more compressed toward the plane due to the pressure provided by a large magnetic field (e.g., Babel & Montmerle 1997). However, this cannot be the full story because the most relevant quantity, the ratio "η" of magnetic to wind energy densities is actually larger for 36 Lyn than for σ Ori E and yet the disk of the former has a somewhat larger height (Smith et al. 2006). Might other considerations, such as the larger radial extent of the disk (e.g. in the case of 36 Lyn), have a bearing on this question?

In addition to these dimensional properties, we find that a phase discrepancy of +0.018 cycles exists between the phase at which the central absorption transits the center of the hydrogen line and the phase of EW maximum. This agrees with a similar phase difference found by GH77 and calls into definition of the star's period when determined from different observation modes. The secondary occultation is distinguished by the passage of two weak lobes, the phases of which are consistent with the semi-resolved structure of the light curves in the literature. The interpretation of this structure is not clear, but it may be related to a disk "warping" or a corrugation of the disk plane predicted in the TO05 models.

When we view the disk edge-on through the magnetic plane, the Balmer line absorptions are opaque, and thus the absorptions of the high-level members of this series increase. For H9 the optical depth is about 100, while it is $\approx$10 for H20, and $\approx$2 at the Balmer edge. As the disk ingresses and egresses there is an absence of an absorption tail in the equivalent width curves. This confirms the theoretical expectation (e.g., TO05) that the density scale height is very small compared to the stellar radius. This implies in turn that our homogeneous slab models of the disk and the total mass estimate of about 1×10^{-10} $M_\odot$ are only rough approximations.

How would hypothetical data of indefinitely high quality (signal-to-noise, spectral resolution, and cadence) improve on our analysis of the disk of σ Ori E? We can think of the following applications of enhanced quality data:

One improvement would be in the mapping of vertical density distribution and indeed the separation of the two density maxima associated with the secondary occultation. This would result from tracing details of the absorption subfeatures as they migrate across the line profiles. An improvement in our understanding of the vertical stratification should indirectly improve out understanding of whether the disk is warped and the inner edge of the secondary occultation-causing segment extends almost to the star or not. It will also clarify the cause of the phase delays that both we and GH76 have found among various hydrogen lines and with respect to the continuum. A resolution of this issue would allow an improved determination of ephemerides from flux curves derived from different diagnostics, thereby leading to a definitive determination of the period and perhaps its first derivative.

Second, the changes in the highest-level lines detected during the ingress and egress of the occultations can be used in principle to further map the vertical density distribution of the disk segments because of the different optical depth regimes in which the various lines are formed.

Third, highly accurate difference profiles should allow one to search for asymmetric absorption features in the EW curves that could indicate the rate at which disk particles leak from the disk either through the inner or outer edge.

Fourth, increased data quality improvements (assuming a stable spectrograph and atmospheric transmission) can lead to the observation of subtle changes in disk structure. We suggest that these might occur on timescales of one to a few months or longer. Finding such changes could allow one ultimately to correlate them with the expected "break out" of disk matter through the outer edge (ud-Doula et al. 2006), possibly associated with X-ray flares from this star (Groote & Schmitt 2004; Sanz-Forcada et al. 2004).

Acknowledgements. The authors are indebted to Drs. Detlef Groote and Rich Townsend for key discussions on phase discrepancies and surface inhomogeneities that improved the quality of this work. D.A.B. also thanks Dr. Dmitry Monin for conducting the critical primary occultation phase observations of σ Ori E on the final night of the observing run.

References

Babel, J., & Montmerle, T. 1997, A&A, 323, 121
Bagnulo, S., Cabanac, R., Jehin, E., et al. 2006, The UVES Paranal Observatory Project, http://www.sc.eso.orgsantiagouvespopfield_stars_uptonow.html
Berger, J. 1956, Contr. Inst. Ap. Paris, Ser. A, 217
Bohlender, D. A., Brown, D. N., Landstreet, J. D., et al. 1987, ApJ, 323, 325
Bolton, C. T., Fullerton, A. W., Bohlender, D. A., et al. 1986, The Physics of Be Stars, ed. A. Slettebak, & T. P. Snow (Cambridge: Cambridge Univ. Press), 82
Bolton, C. T. 1994, Ap. & Sp. Sci., 221, 95
Crowther, P. A., & Lennon, D. J. 2006, A&A, 446, 279
Groote, D. 2003, Magnetic Fields in O, B, and A Stars, ed. L. Balona, et al., ASP Conf. Ser., 205, 243
Groote, D. 2007, priv. commun.
Groote, D., & Hunger, K. 1976, A&A, 52, 303 (GH76)
Groote, D., & Hunger, K. 1977, A&A, 56, 129 (GH77)
Groote, D., & Hunger, K. 1982, A&A, 116, 64
Groote, D., & Hunger, K. 1997, A&A, 319, 250
Groote, D., & Schmitt, J. H. 2004, A&A, 418, 235
Hesser, J. E., Moreno, H., & Ugarte, P. 1977, ApJ, 210, L31

Hubeny, I., & Heap, S. R. 1996, ApJ, 470 1144
Hubeny, I., Lanz, T., & Jeffery, S. 1994, Newslett. Anal. Astron. Spetra, 20, 30
Hunger, K., Heber, U., & Groote, D. 1989, A&A, 224, 57
Inglis, D. R., & Teller, E. 1939, ApJ, 90, 439
Khokhlova, V. L., Vasilchenko, D. V., Stepanov, V. V., & Romanyuk, I. I. 2000, Ast. Let., 26, 177
Krtička, J., Kubát, J., & Groote, D. 2006, A&A, 460, 145
Krtička, J., Mikulášek, Z., Zverko, J., & Žižňovský, J. 2007, A&A, 470, 1089
Kurucz, R. L. 1993, ATLAS9 Stellar Atmospheres and 2 km s^{-1} Grids, Kurucz CD-ROM #13
Landstreet, J. D., & Borra, E. F. 1978, ApJ, 224, L5
Lanz, T., & Hubeny, I. 2007, ApJS, 169, 83
Lesh, J. R. 1968, ApJS, 17, 371
Oksala, M., & Townsend, R. H. D. 2007, Active OB stars: Laboratories for Stellar & Circumstellar Physics, ed. S. Stefl, et al., ASP Conf. Ser., 361, 476
Osmer, P., & Peterson, D. M. 1974, ApJ, 187, 117
Preuss, O., Schüssler, M., Holzwarth, V., et al. 2004, A&A, 417, 987
Reiners, A., Stahl, B., Wolf, B., et al. 2000, A&A, 363, 585 (R00)
Sanz-Forcada, J., Franciosini, E., & Pallavicini, R. 2004, A&A, 421, 715
Shore, S. N. 1987, AJ, 94, 731
Short, C. I., & Bolton, C. T. 1994, Pulsation, Rotation, & Mass Loss in Early-Type Stars, ed. L. Balona, et al. (Noordwijk: Kluwer), 171
Smith, M. A., & Groote, D. 2001, A&A, 372, 208 (SG01)
Smith, M. A., Wade, G. A., Bohlender, D. A., & Bolton, C. T. 2006, A&A, 458, 581
Townsend, R. D. T. 2007, priv. commun.
Townsend, R. D. T., & Owocki, S. P. 2005, MNRAS, 357, 215 (TO05)
Townsend, R. D. T., Owocki, S. P., & Groote 2005, ApJ, 630, L81 (TOG05)
ud-Doula, A., Townsend, R. H. D., & Owocki, S. P. 2006, ApJ, 640, L191
Walborn, N. R. 1974, ApJ, 191, L95